applied optics

Parametric dog-bone-shaped tunable cylindrical fluidic lens

Erol Ozgur,[1,*] Daniel Reetz,[2] Farhad Akhoundi,[1,2] Nicholas O'Brien,[2] Jaclyn Wycoff,[1,2] Ram Voorakaranam,[2] Pierre-Alexandre Blanche,[1] Lloyd LaComb,[1,2] Chen Liang,[2] Gholam Peyman,[1,2] and N. Peyghambarian[1,2]

[1]James C. Wyant College of Optical Sciences, University of Arizona, Tucson, Arizona 85721, USA
[2]ICRX Inc., Tucson, Arizona 85705, USA
*Corresponding author: erol@optics.arizona.edu

Received 10 March 2021; revised 9 May 2021; accepted 9 May 2021; posted 11 May 2021 (Doc. ID 424659); published 27 May 2021

Tunable spherical fluidic lenses are among the most essential components in adaptive optics. However, fabricating cylindrical tunable lenses has proven more challenging, mainly due to the difficulty in eliminating the defocus component. We demonstrate a parametric approach to minimize the defocus in cylindrical tunable fluidic lenses. We theoretically model and experimentally verify that a dog-bone-shaped tunable cylindrical fluidic lens exhibits almost pure cylindrical performance within the range of ±5D of astigmatism. We anticipate these results will facilitate the use of tunable cylindrical fluidic lenses in adaptive optics applications and particularly ophthalmic devices, where rapid and reliable wavefront correction is required.

https://doi.org/10.1364/AO.424659

1. INTRODUCTION

Tunable lenses are frequently used in zoom systems or adaptive optics applications. They enable focusing, as well as correct for optical aberrations without the need for complex designs and bulky optical systems. Various strategies have been employed to fabricate tunable optical lenses with different characteristics. Tunable fluidic lenses, which are mainly used for inducing defocus or correcting spherical aberrations [1], are one of the earliest and most commonly used examples of tunable lenses. They exploit the pressure change in the liquid inside the lens, which changes the shape of an elastic and transparent membrane to refract transmitted light [2]. The architecture could contain two compartments for the lens and the reservoir [3], or a single compartment where the fluid volume is tuned using an electromagnetic voice coil [4]. There have been several other methods for fabricating tunable lenses demonstrated in the literature, such as tunable polymer lenses [5], liquid crystal lenses [6], piezoelectric tunable lenses [7], and multimaterial systems including liquid trapped in silicone elastomer [8], or two-liquid combination [9]. However, tunable fluidic lenses offer advantages over the other approaches particularly in terms of aperture size and polarization-independent broadband transmission. Other alternatives for tunable lenses in adaptive optics are deformable mirrors [10], which are not see-through and also have a more oscillatory behavior in their operation cycles compared to the tunable lenses [11] and spatial light modulators, which are mainly limited to microscopy applications [12].

Spherical fluidic lenses that produce almost no higher-order monochromatic aberrations are commercially available. Adaptive spherical lenses continue to be an active research area with improvement in spherical lenses to control chromatic aberrations, and theoretical [13] and experimental work to create tunable aspherical lenses [14]. The relative ease of spherical lens fabrication derives from the fact that a simple circular aperture is adequate to fabricate a tunable fluidic lens [15]. To have a cylindrical tunable lens that does not induce defocus or other optical aberrations requires a rectangular aperture with an infinite length, which is not practical. Rectangular flexible membranes having an aspect ratio larger than 3:1 provide a reasonable cylindrical lens-like effect; yet, they have some inherent defocus, which causes a significant deviation from a perfect cylindrical lens even if the clear apertures is small compared to the physical dimension of the membrane [15]. Fabricating cylindrical tunable lenses that do not contain further monochromatic aberrations therefore constitutes a serious challenge in adaptive optics. There are a limited number of examples in the literature of tunable cylindrical lenses such as tubular lenses [16] and dielectric elastomer actuators [17]. These cylindrical lenses exhibit a constant defocus, which limits their usefulness. There is also a theoretical study about a liquid core cylindrical lens that does not possess any spherical aberration [18]; although, the experimental verification of that design was not included in the study.

Modifying the flexible aperture geometry was demonstrated by Stürmer *et al*. [19] as an alternative method for improving the characteristics of the cylindrical lens, in terms of reducing

the defocus effect. They used a dog-bone shape that has wedges at the corners, and they reported two different aperture sizes in their study. This method for creating a cylindrical lens reduces the less defocus compared to previous examples, yet the study does not discuss the mechanism for this improvement. Thus, the lack of a systematic approach for the fabrication of robust and reliable cylindrical tunable lenses is still an impediment to developing adaptive optics tools and devices, particularly in ophthalmology. Current examples of ophthalmologic diagnostic tools, including adaptive optics elements, contain a spherical tunable lens and a pair of rotary cylindrical lens that increase the cost and complexity of the system [20]. The adaptive optical elements enable the development of automated measurement systems controlled by feedback loops, which do not require user input, therefore saving time, resources, and energy. Developing a general solution for the fabrication of cylindrical lenses free of spherical aberrations would be an important achievement in adaptive optics.

In this study, we systematically investigated a parameterized dog-bone shape using finite element model (FEM) analysis to understand its improvement over the rectangular geometry and find the parameters that create the minimum defocus in the lens. After optimizing the design, we fabricated these lenses and measured the refractive characteristics of the lenses using a Shack–Hartmann wavefront sensor (SHWS). The results show that the parametrically designed dog-bone shape could be used for the fabrication of cylindrical lenses with almost pure cylindrical characteristics.

2. FINITE ELEMENT ANALYSIS STUDIES

We have developed a parametric model for the dog-bone shape and tested the effect of stretching on these shapes using finite element analysis (FEA), using COMSOL software. The shape was based on a rectangle with a length-to-width aspect ratio of 3:1. We chose the width (w) and the length (l) of the rectangle as 16 and 48 mm, to have the minimum possible size of the fluidic lens, while simultaneously matching the clear optical aperture size of commercial tunable fluidic lenses [21], which is 16 mm. The parametrization is schematically described in Fig. 1.

The dog-bone-shaped deviation from the rectangle was defined using two circles, to parametrize the radius of the inward ($r1$) and outward ($r2$) curves of the dog bone. The nomenclature for the parametric dog-bone shape was structured as **dogbone(r1, r2)**. The longitudinal portion of the dog bone was divided into three sections,

$$\begin{aligned}
&\text{I) } x < \frac{l}{2} - r1 - 2r2 \text{ (flat region)},\\
&\text{II) } \frac{l}{2} - r1 - 2r2 < x < \frac{l}{2} - 2r2 \text{ (inward curve)},\\
&\text{III) } x > \frac{l}{2} - 2r2 \text{ (outward curve)},
\end{aligned} \tag{1}$$

where the function $y = f(x)$ for drawing the dog-bone shape with respect to the regions is given as

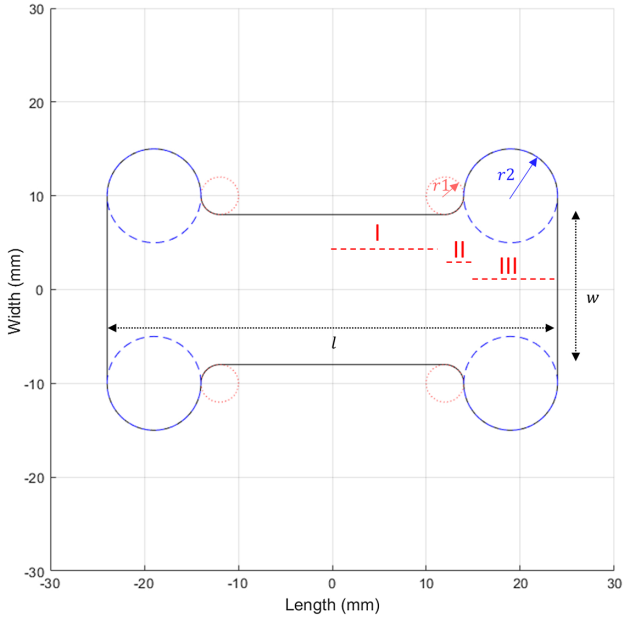

Fig. 1. Parametrization of the dog-bone shape for the FEA studies. The dog-bone shape is formed by using two circles to define the inward and outward curvatures of the flexible membrane. There are four parameters in our study, which are the width (w) and the length (l) of the initial rectangle, and the radii of the curvature ($r1$ and $r2$) of the defining circles. The drawing of the curved side was performed by separating it into three regions, each region having a separate function. In the simulations, fixed values of 16 and 48 mm were used for w and l. Each dog-bone shape is denoted using the $r1$ and $r2$ values, as **dogbone(r1, r2)**.

Table 1. Parameters Used in FEA Simulations

Material	Modulus of Elasticity	Poisson's Ratio	Density	Thickness	Applied Pressure
PDMS	70 MPa	0.495	970 kg/m^3	0.1651 mm	1 kPa

$$\begin{aligned}
&\text{I) } y = \frac{w}{2},\\
&\text{II) } y = \frac{w}{2} + r1 - \sqrt{r1^2 - (x - (l/2 - 2r2 - r1))^2},\\
&\text{III) } y = \frac{w}{2} + r1 + \sqrt{r2^2 - (x - (l/2 - r2))^2},
\end{aligned} \tag{2}$$

and this parametrization is extrapolated to the other three corners by using the symmetries in a rectangle.

Once the parametrization was defined, the FEA simulations were performed using the parameters given in Table 1. These parameters were either obtained from the manufacturer of silicone elastomers (Gel-Pak) that were used in the fabrication step or assumed to be the same as polydimethylsiloxane (PDMS), which is a closely related silicone elastomer.

The elastomer geometry was defined as a parametric dog-bone shape, and the morphological changes under applied pressure were investigated. During the FEA studies, a rectangular shape was also modeled and simulated for comparison with rectangular cylindrical fluidic lenses [Figs. 2(a) and 2(b)]. For the modeling studies, the flatness of a square area at the center

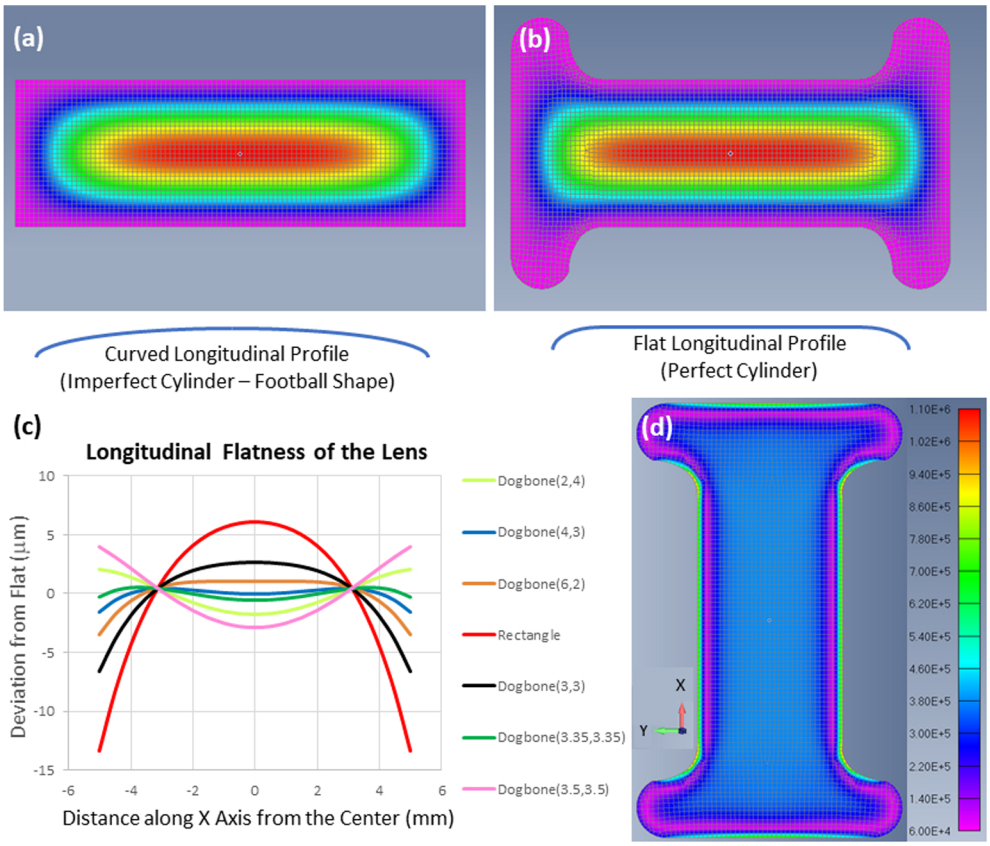

Fig. 2. FEA studies for the parametric dog-bone shape. (a) A rectangular shape was modeled initially and used as a reference. (b) Dog-bone shapes of various parameters were modeled, and the effect of applied uniform pressure of 1 kPa is investigated on the model. (c) The longitudinal profile provides the information about the defocus characteristics of the fluidic lens. The best purely cylindrical performance is obtained when the curve has the flattest response in the longitudinal direction. In the graph, six different parameter sets, some of which $r1 = r2$, are shown together with the rectangular lens. The samples chosen were among the dog-bone shapes that have the closest approximation to a flat profile. (d) Detailed stress analysis of the dog-bone shape. The stress boundary is accumulated towards the dog-bone edges; therefore, stress is distributed evenly around the center of the lens.

of the flexible membrane with a length and width of 10 mm was considered. The impact of other phenomena such as material creep was neglected in the evaluation.

The most important finding of the FEA study was that the rectangular shape had a curved longitudinal profile over the entire aperture, which created an imperfect cylinder. On the other hand, the dog-bone shape enabled a flatter longitudinal profile over 10 mm of clear aperture. Several parameter sets enabled close to flat longitudinal profile for the elastomer, which are given in Fig. 2(c).

A detailed stress analysis [Fig. 2(d)] shows why the dog-bone shape creates a more ideal cylindrical lens compared to a rectangular shape. As can be seen from the figure, the dog-bone shape shifts the stress boundary to be accumulated at the edges of the dog bone, therefore enabling a uniform stress distribution towards the center. This results in a fluidic lens that resembles a pure cylindrical lens, particularly in the center clear aperture.

3. DOG-BONE CYLINDRICAL LENS FABRICATION AND CHARACTERIZATION

We fabricated a cylindrical lens system consisted of two reciprocal cylindrical lenses on opposite sides of an aluminum container, having a 45° tilt between them (Fig. 3). This design was preferred, since it previously demonstrated correction of cylindrical aberrations with all possible axes of cylinder [22] while leaving a large opening in the center when used in a binocular system. Although we used a systematic approach for determining the dog-bone-shaped lens parameters $r1$ and $r2$, we did not observe a significant pattern related to these parameters. There were several models that approached a flat longitudinal profile [Fig. 2(c)]. We used the design version **dogbone(3.35,3.35)**because it was among the designs having a minimum amount of deviation from a flat longitudinal profile [see Fig. 2(c)] and included a single parameter instead of two, thus simplifying the design. The two lenses were separated by a glass window, and each lens had independently controlled reservoirs of liquid connected to the lenses by polymer tubing. The volume of the reservoirs could be changed using stepper motors, controlled by custom software. Gel-Pak silicone elastomer with a thickness of 6.5 mils (≈165 μm) was used as the flexible material; both the fluidic lens and the reservoirs were filled with mineral oil.

A custom-built auto refractometer was used to characterize the dog-bone cylindrical lenses. A fiber-coupled LED and a Thorlabs F810FC-780 collimator produced a collimated beam

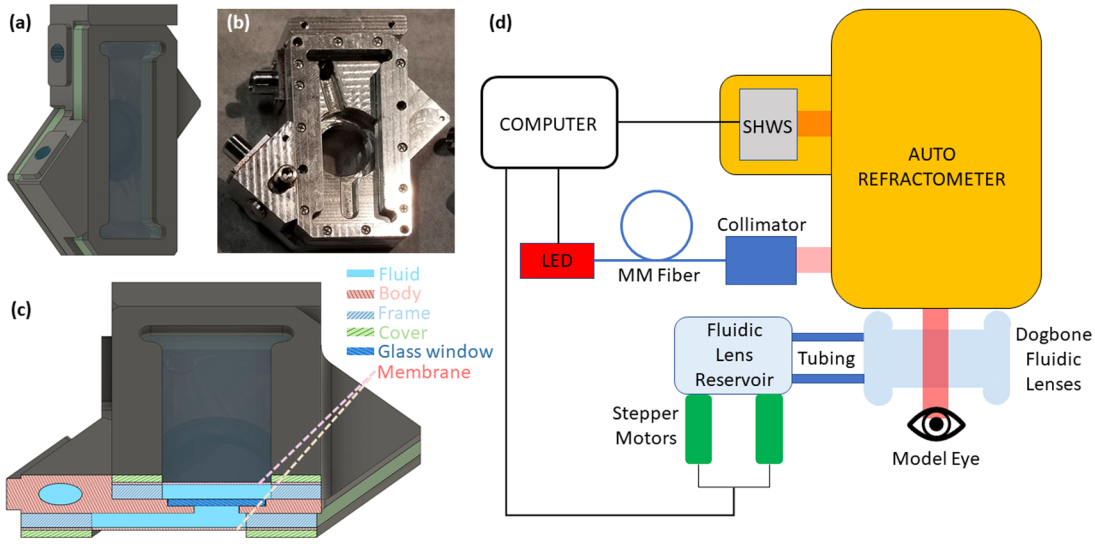

Fig. 3. Fabricated dog-bone cylindrical lens and the optical characterization setup. (a) CAD drawing of the cylindrical lens system that was fabricated; (b) fabricated dog-bone lens body; (c) CAD representation of the lens cross section. A flexible silicone elastomer is held between a dog-bone-shaped aluminum frame and cover, which is mounted on an aluminum body. Two lenses sharing a common circular aperture with a diameter of 16 mm are fabricated on the reciprocal sides of the body, at a 45° angle. A glass window separates the lenses. Each lens is separately connected to a reservoir with polymer tubing. The volumes of the reservoirs are altered using stepper motors. The fluidic lenses were filled with mineral oil as the fluid. (d) The optical setup used for lens characterization. The dog-bone fluidic lenses were incorporated into a custom-built autorefractometer that measures the refractive error of the eye. A collimated beam obtained from a multimode (MM) fiber-coupled LED is scattered back from a model eye that has diffuse reflection characteristics. The scattered light passes through the dog-bone fluidic lenses and then the autorefractometer, which relays the image of the model eye pupil onto an integrated SHWS. The SHWS calculates the Zernike coefficients of the incoming light and reports the deviation from a planar wavefront.

at 820 nm. The beam was directed towards a model eye, which is a retroreflector consisting of a focusing element and a diffuse reflector at the focal point. The cylindrical fluidic lenses were used to induce astigmatism in the model eye, which was otherwise tuned to scatter a plane wavefront. The light scattered from the back of the reflector passes through the fluidic lenses and the auto refractometer optical elements, which relays the image at the pupil of the model eye onto an integrated Thorlabs WFS30-5C SHWS having a Thorlabs MLA150-5C microlens array with a focal length of 4.1 mm. The SHWS, using its internal calibration, measures the optical aberrations of the incoming wavefront and calculates the corresponding Zernike coefficients. In this study, we considered the spherical and cylindrical aberrations that are defined using the three Zernike coefficients, $Z3$, $Z4$, and $Z5$. We used the ANSI Z80.28 standard for reporting the Zernike values [23]. The lenses were mounted horizontally (optical axis vertical) to minimize the effect of the gravitational sagging [24]. The two cylindrical lenses were measured separately. While one lens was being measured, the second lens was kept at the zero diopter position.

4. RESULTS AND DISCUSSION

The measurements of the Zernike coefficients demonstrate that the vertically aligned lens exhibits a significant change in the $Z5$ and $Z4$ coefficients with respect to the motor motion [Fig. 4(a)], while the 45° tilted lens mainly affects the $Z3$ and $Z4$ coefficients [Fig. 4(c)]. This is an expected result because $Z5$ is associated with astigmatism at 0°, while $Z3$ is related to 45° [25]. The $Z4$ contribution is due to the fact that these two Zernike coefficients are also related to defocus [26]; however, this does not add any additional spherical aberration to the dog-bone-tunable cylindrical fluidic lens [Figs. 4(b) and 4(d)]. The measured cylinder diopter values were also compared to a cylindrical lens model having the same volume and refractive index, and the calculations showed good agreement with the experiments. Both lenses show a large tunability, ±5D in cylindrical optical power. This is particularly important for ophthalmologic applications, since the prevalence of astigmatism larger than 5D is less than 1% [27].

One common issue with the fluidic lenses is gravitational sagging, which manifests itself as vertical coma [28], represented with the $Z7$ in the Zernike ANSI notation [23]. We investigated the effect of the gravity sag in the dog-bone cylindrical lenses by measuring the variation of $Z7$ in horizontal and vertical optical axis orientations for 0° [Fig. 5(a)] and 45° [Fig. 5(b)] lenses. Both lenses had a constant $Z7$ value over a large diopter range, which diminished when the optical axis was converted to vertical; therefore, the fluidic lenses will perform better when they are mounted horizontally. We calculated the Bond number of the fluidic lens, using the membrane stiffness in lieu of the surface tension. Since it is a focus tunable lens, the Bond number varies with the radius of curvature. Within a range of ±5D, we found that the Bond number is smaller than 1, except when the lens membrane is close to being flat (±0.25D). This shows that gravity has an overall minimal effect on the fluidic lens.

Another effect that must be considered while operating fluidic lenses is thermal expansion [29]. Figure 5(c) shows the effect of the temperature on $Z3$ and $Z5$. Here, the fluidic lenses

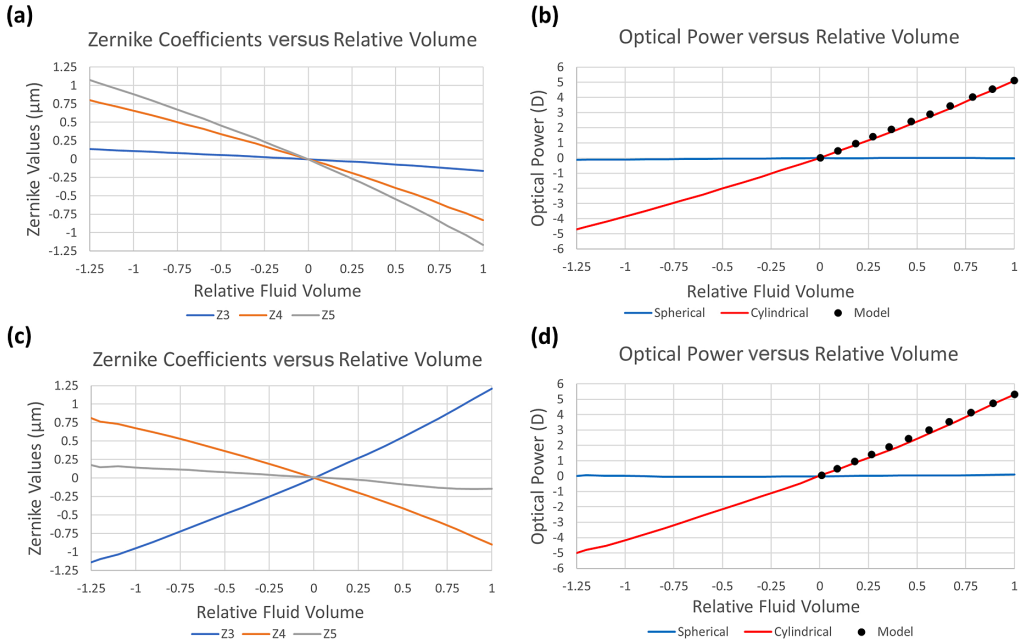

Fig. 4. Measurements of the dog-bone-tunable cylindrical fluidic lenses. (a) Measured Zernike coefficients and (b) optical power in diopters of the 0° lens; (c) measured Zernike coefficients and (d) optical power in diopters of the 45° lens. The black dots represent the calculated diopter value that is obtained when a cylindrical lens having the same volume and refractive index is modeled. $R^2 > 0.99$ is obtained in both fits. The measurements were represented as values versus the relative fluid value that is infused into, or withdrawn from, the lens using the stepper motors, which control the reservoir volume. ANSI Z80.28 standard was used to represent the Zernike coefficients [23], where $Z3$, $Z4$, and $Z5$ represent 45° astigmatism, defocus, and 0° astigmatism, respectively [25].

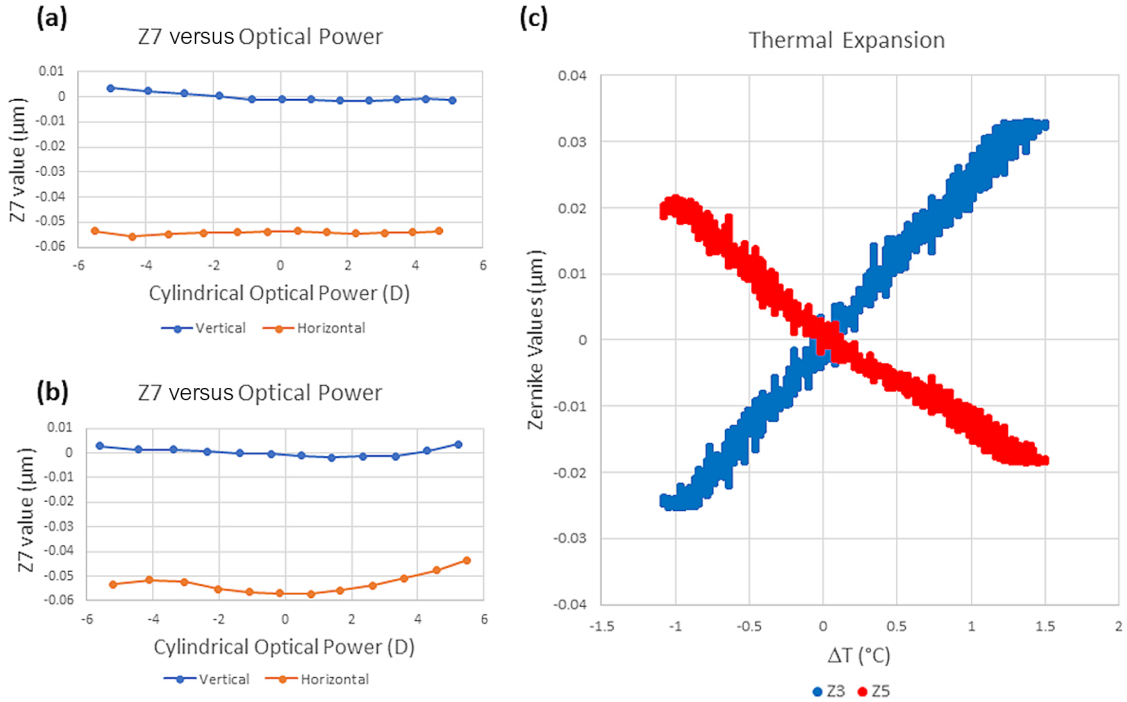

Fig. 5. Gravity sagging and thermal characterization of the dog-bone cylindrical lens assembly. (a) $Z7$ component in the Zernike coefficients of the 0° lens when the lens is assembled in an optically vertical (blue) and horizontal (orange) orientation; there is a noticeable increase in the absolute $Z7$ value in the horizontal optical axis orientation, which is associated with the vertical coma. (b) The same effect is observed with the 45° lens. In both lenses, the value of $Z7$ remained constant on a large diopter range. (c) Effect of the temperature change on the Zernike coefficients associated with the astigmatic aberration. The deviation in the Zernike values with respect to ΔT is almost linear ($R^2 > 0.95$), and it is not very significant.

were set to zero position, and the change of the Zernikes with respect to the temperature were measured, using a thermometer attached to the fluidic lens body, and thermally insulated from the environment using foam. As can be seen from the figure, the effect of thermal expansion on the fluidic lens system is not very dramatic (0.05 over a temperature range of 2.5°C), and it is also linear, which can be compensated mathematically. Finally, the response time of these fluidic lenses is limited to the characteristics of the stepper motors. In our system, we measured a response time of 2.5 D/s. This value is anticipated to be adequate for ophthalmologic applications in particular.

In this study, we demonstrate a parametric approach to fabricate dog-bone-shaped tunable cylindrical fluidic lenses and systematically investigated the parameter space to identify the optimal configuration. The number of the parameters was kept as small as possible; nevertheless, one of the best results was obtained using only a single radius of curvature parameter, besides the length and the width of the rectangle that the dog-bone shape is based on. We then fabricated a cylindrical fluidic lens system that contains two reciprocal cylindrical lenses. It is also possible to include other parameters to make the parametric design even more versatile, such as a difference in the y position of the circle centers that define the inward and outward curve and ellipticity in these circles. Yet, the performance of the dog-bone-shaped cylindrical lenses with three parameters is quite effective.

We did this research mainly to find the best parameters that would yield the purest cylindrical characteristics in a tunable cylindrical fluidic lens. Some of the parameters, such as the thickness of the membrane, were chosen according to the materials that were planned to be used in our fabrication. Changes in these materials may affect the model. For example, we also modeled a membrane that has 120 μm thickness instead of 165 μm. We measured the ratio of deviation from a longitudinal profile as 1.14, instead of 1.38, the value that would be observed from a linear system having the same magnitude of tension. Therefore, it seems that there is a nonlinear relation between the membrane thickness, and possibly the other membrane properties, with the lens characteristics. Another topic that can be further investigated is to establish a general relation between the geometrical parameters and the amount of convergence towards a pure cylindrical lens. Our research suggests that all these questions may be addressed by applying FEA to the problem, which is beyond the scope of our work.

In conclusion, the dog-bone shape, which characteristics were determined using a parametric approach, is significantly superior to rectangular cylindrical lenses. The output of this research is expected to pave the way for adaptive optics components and ophthalmologic instruments that measure and correct for optical aberrations, relying on tunable fluidic lens systems alone.

Acknowledgment. This study was funded by ICRX Inc. The authors would like to thank Daniel Hofstadter for valuable discussions on the FEA.

Disclosures. EO, ICRX, Inc. (F,P); DR, ICRX, Inc. (C,P); FA, ICRX, Inc. (E,P); NO, ICRX, Inc. (E); JW, ICRX, Inc. (E); RV, ICRX, Inc. (E); P-AB, ICRX. Inc. (S); LL, ICRX, Inc. (E); CL, ICRX, Inc. (S); GP, ICRX, Inc. (I,P,S); NP, ICRX, Inc. (I,P,S).

Data Availability. Data underlying the results presented in this paper are not publicly available at this time but may be obtained from the authors upon reasonable request.

REFERENCES

1. D. Y. Zhang, N. Justis, and Y. H. Lo, "Integrated fluidic adaptive zoom lens," Opt. Lett. **29**, 2855–2857 (2004).
2. G. A. Peyman, "External lens adapted to change refractive properties," U.S. patent 7,993,399 (27 July 2011).
3. N. Savidis, G. Peyman, N. Peyghambarian, and J. Schwiegerling, "Nonmechanical zoom system through pressure-controlled tunable fluidic lenses," Appl. Opt. **52**, 2858–2865 (2013).
4. D. Niederer, "Liquid lens system," European patent EP2176691B1 (8 June 2011).
5. G. Beadie, M. L. Sandrock, M. J. Wiggins, R. S. Lepkowicz, J. S. Shirk, M. Ponting, Y. Yang, T. Kazmierczak, A. Hiltner, and E. Baer, "Tunable polymer lens," Opt. Express **16**, 11847–11857 (2008).
6. P. Valley, D. L. Mathine, M. R. Dodge, J. Schwiegerling, G. Peyman, and N. Peyghambarian, "Tunable-focus flat liquid-crystal diffractive lens," Opt. Lett. **35**, 336–338 (2010).
7. Y. Zou, W. Zhang, F. S. Chau, and G. Zhou, "Miniature adjustable-focus endoscope with a solid electrically tunable lens," Opt. Express **23**, 20582–20592 (2015).
8. C. Fang, B. Dai, R. Zhuo, X. Yuan, X. Gao, J. Wen, B. Sheng, and D. Zhang, "Focal-length-tunable elastomer-based liquid-filled plano-convex mini lens," Opt. Lett. **41**, 404–407 (2016).
9. J. H. Wang, W. P. Tang, L. Y. Li, L. Xiao, X. Zhou, and Q. H. Wang, "Hybrid driving variable-focus optofluidic lens," Opt. Express **27**, 35203–35215 (2019).
10. I. Kanno, T. Kunisawa, T. Suzuki, and H. Kotera, "Development of deformable mirror composed of piezoelectric thin films for adaptive optics," IEEE J. Quantum Electron. **13**, 155–161 (2007).
11. C. Dorronsoro, X. Barcala, E. Gambra, V. Akondi, L. Sawides, Y. Marrakchi, V. Rodriguez-Lopez, C. Benedi-Garcia, M. Vinas, E. Lage, and S. Marcos, "Tunable lenses: dynamic characterization and fine-tuned control for high-speed applications," Opt. Express **27**, 2085–2100 (2019).
12. C. Maurer, A. Jesacher, S. Bernet, and M. Ritsch-Marte, "What spatial light modulators can do for optical microscopy," Laser Photon. Rev. **5**, 81–101 (2011).
13. P. Zhao, C. Ataman, and H. Zappe, "Spherical aberration free liquid-filled tunable lens with variable thickness membrane," Opt. Express **23**, 21264–21278 (2015).
14. H. Zhou, X. Zhang, Z. Xu, P. Wu, and H. Yu, "Universal membrane-based tunable liquid lens design for dynamically correcting spherical aberration over user-defined focal length range," Opt. Express **27**, 37667–37679 (2019).
15. R. Marks, D. L. Mathine, J. Schwiegerling, G. Peyman, and N. Peyghambarian, "Astigmatism and defocus wavefront correction via Zernike modes produced with fluidic lenses," Appl. Opt. **48**, 3580–3587 (2009).
16. D. Kopp and H. Zappe, "Tubular astigmatism-tunable fluidic lens," Opt. Lett. **41**, 2735–2738 (2016).
17. M. Ghilardi, H. Boys, P. Török, J. J. C. Busfield, and F. Carpi, "Smart lenses with electrically tuneable astigmatism," Sci. Rep. **9**, 16127 (2019).
18. L. Sun, S. Sheng, W. Meng, Y. Wang, Q. Ou, and X. Pu, "Design of spherical aberration free liquid-filled cylindrical zoom lenses over a wide focal length range based on ZEMAX," Opt. Express **28**, 6806–6819 (2020).
19. M. Stürmer, A. Schatz, and U. Wallrabe, "Cylindrical lens with integrated piezo actuation for focal length tuning and lateral scanning," in *IEEE 27th International Conference on Micro Electro Mechanical Systems (MEMS)* (2014), pp. 1171–1174.
20. S. Boutinon, V. T. Del Rio, and M. Nauche, "Phoropter, and method for measuring refraction using a phoroptor of said type," international patent WO2,015,155,458 (2 February 2017).
21. W. A. Torres-Sepúlveda, J. D. H. Escobar, J. A. M. Marín, A. Mira-Agudelo, and E. A. R. Muñoz, "Hysteresis characterization of an electrically focus-tunable lens," Opt. Eng. **59**, 044103 (2020).

22. B. Amirsolaimani, G. Peyman, J. Schwiegerling, A. Bablumyan, and N. Peyghambarian, "A new low-cost, compact, auto-phoropter for refractive assessment in developing countries," Sci. Rep. **7**, 7 (2017).
23. ANSI, "Ophthalmics: methods of reporting optical aberrations of eyes | engineering 360," ANSI Z80.28, 2017.
24. P. Zhao, C. Ataman, and H. Zappe, "A miniaturized adaptive-focus camera objective employing a gravity-immune liquid-tunable aspherical lens," Proc. SPIE **10116**, 101160C (2017).
25. V. Lakshminarayanan and A. Fleck, "Zernike polynomials: a guide," J. Mod. Opt. **58**, 545–561 (2011).
26. J. C. Wyant and K. Creath, "Basic wavefront aberration theory for optical metrology," Appl. Opt. Opt. Eng. **11**, 1–53 (1992).
27. H. C. Fledelius and M. Stubgaard, "Changes in refraction and corneal curvature during growth and adult life," Acta Ophthalmol. **64**, 487–491 (1986).
28. D. Kopp and H. Zappe, "Tubular focus-tunable fluidic lens based on structured polyimide foils," IEEE Photon. Technol. Lett. **28**, 597–600 (2016).
29. X. Hu, G. Wang, Y. Zhang, H. Yang, and S. Zhang, "Large depth-of-field 3D shape measurement using an electrically tunable lens," Opt. Express **27**, 29697–29709 (2019).